Droplet Interactions in Water-in-Carbon Dioxide Microemulsions Near the Critical Point: A Small-Angle Neutron Scattering Study

C. T. Lee, Jr.,[†] K. P. Johnston,*[,†] H. J. Dai,[‡] H. D. Cochran,[‡,§] Y. B. Melnichenko,[||] and G. D. Wignall*[,||]

Department of Chemical Engineering, University of Texas at Austin, Austin, Texas 78712, Department of Chemical Engineering, University of Tennessee, Knoxville, Tennessee 37996, and Chemical Technology and Solid State Divisions, Oak Ridge National Laboratory, Oak Ridge, Tennessee 37831

Received: September 16, 2000; In Final Form: January 29, 2001

Droplet interactions in water-in-carbon dioxide (W/C) microemulsions formed with a perfluoropolyether-based surfactant for droplet volume fractions from 0.05 to 0.10 are studied with small-angle neutron scattering (SANS) to understand the mechanism of microemulsion stability. The water-to-surfactant ratio (W_o) is fixed at 12.5. Droplet interactions increase as the upper critical solution pressure is approached with decreasing pressure at constant temperature, increasing temperature at constant pressure, or increasing droplet volume fraction. These interactions are quantified in terms of the structure factor at zero momentum vector, $S(0)$, and the correlation length, ξ, for an Ornstein−Zernicke structure factor, or the square-well depth for the structure factor of a square-well potential. Near the critical solution pressure, the interaction strength (A) approaches the value predicted for a hard-sphere fluid with a van der Waals attractive term. The observed interaction strength between droplets is larger in W/C relative to water-in-oil microemulsions due to stronger tail−tail interactions resulting from the weak solvation by CO_2. Overcoming these larger droplet interactions is the key challenge in forming stable W/C microemulsions. Pressure and volume fraction have a negligible effect on the droplet size; however, drop size decreases with temperature.

Introduction

CO_2 as a liquid or supercritical fluid ($T_c = 31$ °C, $P_c = 73.8$ bar) exhibits solvent properties that are tunable with pressure, and it is essentially nontoxic and nonflammable. It is nonpolar (unlike water) and has weak van der Waals forces (unlike oils). Dispersions of water-in-CO_2, whether on the nanometer (microemulsions)[1−4] or micrometer (emulsions)[5] scale, may be utilized as environmentally benign replacements for organic solvents to dissolve both hydrophilic and hydrophobic compounds. These dispersions offer new possibilities for separations on the basis of polarity and as media for chemical reactions,[6−9] as well as the formation of nanoparticles.[10,11]

The existence of a bulk water domain in a water-in-CO_2 (W/C) microemulsion was demonstrated by several spectroscopic techniques with an ammonium carboxylate perfluoropolyether surfactant (PFPE-$COO^-NH_4^+$).[2] Small-angle neutron scattering (SANS) experiments[3,4,12,13] and molecular simulations[14] on this and other systems confirmed the existence of microemulsions with a radius of 20−35 Å spherical water droplets dispersed in CO_2. Percolation of water/PFPE-$COO^-NH_4^+$/CO_2 microemulsion systems was recently studied over a large range of pressures, temperatures, and droplet volume fractions.[15] A nearly 3 orders of magnitude increase in the electrical conductivity was observed as a result of increasing droplet interactions. Scaling analysis of the conductivity behavior supported a dynamic percolation mechanism whereby the increase in droplet interactions gives rise to the formation of clusters of discrete droplets.[16−18] This mode of percolation is in contrast to static percolation, which results in the formation of bicontinuous structures.[16,19]

The ability to form microemulsions in CO_2 depends on interfacial curvature and droplet interactions. For W/C microemulsions, the surfactant geometry must cause the interface to curve about water. The packing parameter $v/a_T l_T$ must be greater than unity, where v is the volume of the surfactant tail region, a_T is the area of the surfactant headgroup at the interface, and l_T is the surfactant tail length. Numerous conventional hydrocarbon surfactants with $v/a_T l_T$ greater than unity have been studied in CO_2; however, these surfactants were incapable of forming W/C microemulsions.[20−22] Thus, this limitation in microemulsion formation is likely a result of attractive interactions between droplets.

SANS has proved to be a valuable technique for studying droplet interactions in conventional water-in-oil microemulsions.[23−26] A strong but short-ranged attractive force arises between the microemulsion droplets due to the overlap of surfactant tails in neighboring droplets.[25,27,28] The strength of droplet interactions increases as solvent−surfactant tail interactions decrease and, accordingly, tail−tail interactions increase.[29,30] Solvation of surfactant tails by CO_2 is often weak, so attractive droplet interactions may be expected to be important. To date, however, SANS experiments on W/C microemulsion systems were performed either on dilute ($\phi < 0.05$) systems, where droplet interactions are less important,[4,12,13] or in regions where only modest changes in droplet interactions were observed.[3]

In the present study, extensive SANS experiments are performed on W/C microemulsions near the critical volume fraction ($\phi_c \sim 0.13$), where droplet interactions are expected to

[†] University of Texas at Austin.
[‡] University of Tennessee.
[§] Chemical Technology Division, Oak Ridge National Laboratory.
[||] Solid State Division, Oak Ridge National Laboratory.

10.1021/jp0033059 CCC: $20.00
Published on Web 04/10/2001

be high. Two models are used to fit the SANS data: a system of polydisperse droplets with an Ornstein−Zernicke structure factor and a system of monodisperse droplets with a square-well potential. The value of the structure factor at zero momentum transfer, $S(0)$, and the correlation length, ξ, in the first model and the square-well depth in the second model are used as quantitative indicators of droplet interactions as a function of pressure, temperature, and droplet volume fraction. The dependence of the square-well depth on the density of CO_2 is studied in an attempt to determine the physical origin of droplet interactions in W/C microemulsions. A better understanding of droplet interactions in W/C versus W/O microemulsions is of primary importance for achieving greater success in designing surfactants for W/C microemulsions. Finally, the results of the fits of the geometric parameters of both models are compared in an attempt to obtain the dimensions of the water core and surfactant tail domains of the microemulsion droplet.

Experimental Section

Materials. An ammonium carboxylate perfluoropolyether surfactant,

$$CF_3-(O-CF_2-CF(CF_3))_n-(O-CF_2)-COO^-NH_4^+$$

was used in all experiments (abbreviated PFPE-$COO^-NH_4^+$). The surfactant had an average molecular weight of 672 g/mol ($n \sim 2.9$) and was synthesized from the acid form (Ausimont, lot D-5) as previously described.[15] Instrument-grade CO_2 (Praxair) and Nanopure II water or deuterated water (99.9 atom %, Aldrich) were used as indicated.

Small-Angle Neutron Scattering. The microemulsions were prepared in a high-pressure, variable-volume view cell equipped with a sapphire window that permitted visual observation of microemulsion formation and phase behavior.[15] A piston inside the view cell was used to vary the pressure independently of temperature. System pressure was controlled with the syringe pump to within 1 bar by using CO_2 as the pressurizing fluid on the backside of the piston, and system temperature was controlled to within ±0.2 °C with heating tape. The cell contents were mixed with a magnetic stir bar inside the cell. The microemulsion cloud point at each concentration was measured by decreasing the pressure from 450 bar until the clear, one-phase microemulsion became cloudy. The variable-volume cell contained two $^5/_8$ in. diameter and $^3/_{16}$ in. thick sapphire windows on opposite sides of the cell along the diameter,[31] resulting in a path length of 22.3 mm.

The SANS data were collected on the W. C. Koehler SANS facility[32] at the Oak Ridge National Laboratory with a 64 × 64 cm^2 area detector and element size ~1 cm^2. The neutron wavelength was $\lambda = 4.75$ Å ($\Delta\lambda/\lambda \sim 5\%$), and the beam at the sample was defined by an 8 mm cadmium iris. The sample−detector distance was 3.3 m and the data were corrected for instrumental backgrounds, detector efficiency, and the scattering from the cell windows for each detector element prior to radial averaging to give a Q range of $0.010 < Q = 4\pi\lambda^{-1} \sin(\theta/2) < 0.185$ Å^{-1}, where θ is the scattering angle. The net intensities were converted to an absolute (±4%) differential cross section per unit sample volume (in units of reciprocal centimeters) by comparison with precalibrated secondary standards, based on the measurement of beam flux, vanadium incoherent cross section, the scattering from water, and other reference materials.[33] The coherent intensities of the sample were obtained by subtracting the (coherent) cross section of CO_2 (~10^{-2} cm^{-1}) and the (incoherent) cross section of the hydrogen atoms (~10^{-3} cm^{-1}) in the surfactant, and these formed only a minor correction to the sample data (<10%) except at higher Q. The transmission through the samples was typically 70%, indicating that multiple scattering can be ignored.[24,26] Scattering curves were collected until the total number of neutrons collected was greater than a given value (300 000), which typically required 5−30 min depending on the droplet concentration and proximity to the cloud point. Conductivity measurements were performed as previously described.[15]

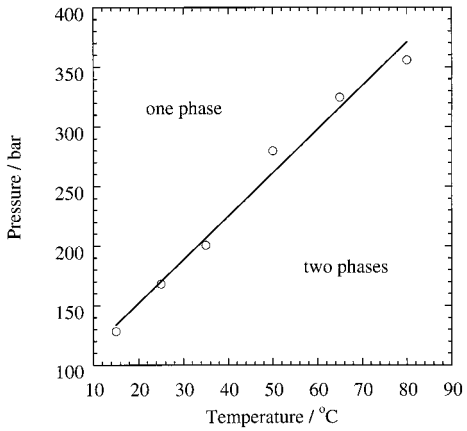

Figure 1. Phase behavior of the D_2O/PFPE-$COO^-NH_4^+$/CO_2 microemulsion system as a function of pressure and temperature at $W_o = 12.5$ and $S/C = 0.15$.

Results and Discussion

Phase Behavior. The phase behavior of D_2O/PFPE-$COO^-NH_4^+$/CO_2 microemulsions is shown in Figure 1. The surfactant to CO_2 mass ratio (S/C) was 0.15 and the moles of water divided by moles of surfactant (W_o) was 12.5, resulting in overall droplet volume fractions of 0.09−0.12. The droplet volume fraction ϕ was calculated as $\phi = \phi_w + \phi_{surf}$, where ϕ_w is the water (H_2O or D_2O) volume fraction and ϕ_{surf} is the surfactant volume fraction calculated from a surfactant density of 1.8 g/cm^3, assuming ideal mixing. The one-phase region is above the curve. As the pressure is lowered at constant temperature, or as the temperature is raised at constant pressure, the microemulsions developed a characteristic orange tinge within 10−20 bar of the cloud point. This tinge indicates an increase in the size of droplets or droplet clusters (to a size that scatters visible light), which may result from increased droplet interactions. After the cloud point was crossed, two phases of similar volumes were observed, the bottom phase having an even deeper orange color than the original one-phase microemulsion system. The similar volumes of the two resulting phases suggests a first-order (e.g., gas → liquid) phase transition,[18] further indicating an increase in droplet interactions as the phase transition is approached.

This first-order transition is illustrated in the CO_2 density−ϕ graphs in Figure 2 where an upper critical solution pressure is observed at a droplet volume fraction of approximately 0.12, which agrees quite well with the prediction of $\phi_c = 0.13$ for a hard-sphere fluid with a van der Waals attractive term. Thus, the phase transition resulting from decreasing the pressure (or increasing the temperature) is likely the result of an increase in interdroplet interactions. This hypothesis is supported by conductivity measurements, where an increase in microemulsion conductivity is observed upon decreasing the pressure or density.[15] At low temperatures (e.g., 10 °C), a critical point is observed upon increasing the pressure, i.e., a lower critical solution pressure. Note that at $\phi = 0.08$, the upper cloud point occurred beyond the maximum experimental pressure. This

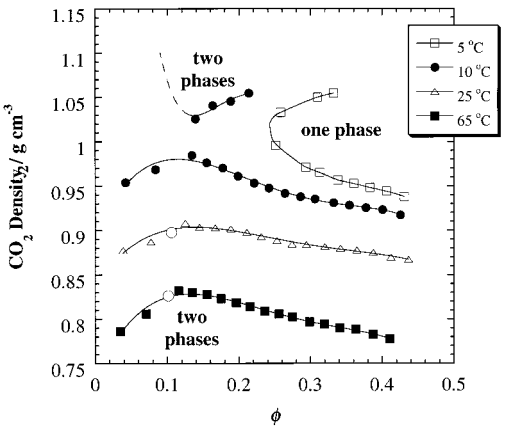

Figure 2. CO_2 density−droplet volume fraction plots at various temperatures. An upper critical solution pressure is observed at all temperatures, while a lower critical solution pressure is also observed at lower temperatures. Open circles are for the D_2O/PFPE-$COO^-NH_4^+$/CO_2 microemulsion system at $W_o = 12.5$ and $S/C = 0.15$, while the other data are for the H_2O/PFPE-$COO^-NH_4^+$/CO_2 microemulsion system at $W_o = 12.5$ and various S/C ratios.

indicates that interdroplet interactions increase as the density of CO_2 is increased, which is supported by the increase in conductivity as the pressure is increased at low temperature.[15] A simple explanation of this phenomenon results by comparing the solubility parameters of the surfactant tail and CO_2. The solubility parameter of the PFPE tails of the surfactant is relatively low with a value of 5.1 $(cal/cm^3)^{1/2}$, while the solubility parameter of CO_2 increases with increasing density from values near zero at gaslike densities to approximately 7.5 $(cal/cm^3)^{1/2}$ at 31 °C and 345 bar. Therefore, at low temperatures and high pressures, the solubility parameter of CO_2 can sufficiently exceed that of the PFPE tails of the surfactant, resulting in a decrease in solvent−tail interactions and an increase in tail−tail interactions and, thus, phase separation resulting from droplet interactions.

Small-Angle Neutron Scattering. To study droplet interactions quantitatively in W/C microemulsions, SANS experiments where performed near the critical volume fraction in Figure 2. The SANS spectra collected as a function of pressure and temperatureare shown in Figures 3−8. The low-Q region of each curve is highlighted, as this is where the droplet interactions are expected to affect the scattering curve. Indeed, as the pressure is reduced at each temperature, an increase in the low-Q scattering is observed, indicating an increase in droplet interactions.[23,24] At 15 °C, the low-Q scattering increases as pressures is lowered or raised from 310 bar, which is likely due to the appearance of a lower critical solution pressure seen in Figure 2 at low temperatures.[15]

To quantify the changes in droplet interactions, the SANS data were fit to two separate models. Details of the first model are given below. The SANS scattering intensity can be written as

$$I(Q) = \phi(\Delta\rho)^2 V_D P(Q,R) S'(Q,R,\phi) \qquad (1)$$

where ϕ is the droplet volume fraction, $\Delta\rho$ is the scattering length density contrast, and V_D is the volume of a single droplet $(=^4/_3\pi R^3)$ with R being the droplet radius. The normalized form factor $P(Q,R)$, which is a function of the droplet size and shape, was calculated by assuming a Schultz distribution of polydisperse spheres with an average droplet radius of R^{avg} and a root-mean-square deviation in droplet sizes of $\sigma = R^{avg}/(Z+1)^{1/2}$ defined by the width parameter Z. This model of the form factor has been applied to both W/C[3,4,12,13] and W/O microemulsions,[23] and typically σ/R^{avg} is approximately 0.25. The structure factor, which depends on the interactions among droplets, was modeled by the modified Ornstein−Zernicke structure factor:

$$S(Q,R,\phi) = 1 + \frac{S(0)}{1 + (Q\xi)^2} \qquad (2)$$

where $S(0) = n_D k_B T \kappa_T$, n_D is the droplet number density, κ_T equals the isothermal osmotic compressibility, and ξ is the correlation length. The effect of droplet polydispersity on the structure factor was taken into account through the use of the modified structure factor $S'(Q) = 1 + \beta(Q)[S(Q) - 1]$, with $\beta(Q)$ given by Kotlarchyk and Chen.[34] Thus, the model included five adjustable parameters, namely, ϕ, R^{avg}, σ/R^{avg}, $S(0)$, and ξ. However, given the relative inaccuracies in determining σ/R^{avg} from the drop-contrast technique employed here (see below) as compared to shell-contrast[35] or contrast-variation[36] techniques, a nominal value of $\sigma/R^{avg} = 0.25$ was used. Allowing σ/R^{avg} to vary in the model fits generally returned $0.2 < \sigma/R^{avg} < 0.3$, with an average value of 0.251, while the remaining parameters in the fit were relatively insensitive to the choice of σ/R^{avg} (typically to within ±5% or better).

The scattering length density difference was calculated by dividing the microemulsion into four regions, namely, bulk D_2O, interfacial D_2O, surfactant tails, and solvent. For W_o values less than about 10, the interfacial water is strongly associated with the surfactant headgroups.[37] The scattering length density of bulk water was calculated from the density of D_2O (1.107 g/cm^3), with the dissolved CO_2 taken into account.[38] The scattering length density of the interfacial water region was calculated from the van der Waals volume of the surfactant headgroup and counterion, with the assumption of 10 mol of water per headgroup. The scattering length density of the surfactant tails was calculated by assuming a surfactant bulk density of 1.8 g/cm^3.[39] Furthermore, solvent penetration into this tail region was accounted for by assuming that 10 CO_2 molecules solvate each surfactant tail.[4,12] The scattering length density of CO_2 was calculated from the bulk density of CO_2 at the given conditions accounting for the solubility of water in CO_2.[40] For all regions above, ΔV_{mix} was assumed to be zero. Values of the scattering length density of bulk water, interfacial water, surfactant tails, and bulk CO_2 calculated from this method were 6.35, 5.23, 2.7−3.2, and 2.0−2.6 ($\times 10^{10}$ cm^{-2}), respectively. Therefore, the primary contrast is between the interfacial water (+surfactant headgroups) and the surfactant tails; thus, the fitted droplet sizes (R_w) and volume fractions (ϕ_w) are for the entire (bulk + interfacial) water region. Note that the regressed values of R_w, $S(0)$, and ξ were insensitive to the value used for the scattering length density contrast, changing by only about 1% as $\Delta\rho$ was allowed to vary by as much as a factor of 2. The primary effect of the choice of $\Delta\rho$ was on the fitted value of ϕ_w, as evident from eq 1. Attempts to model the scattering data with a core and shell model for the form factor failed as the shell thickness always returned zero. This is likely the result of the diffuse nature of the bulk water−interfacial water and surfactant tail−bulk CO_2 boundaries.

The results of the fits of the data to the polydisperse form factor/Ornstein−Zernicke structure factor model are given in Table 1. Excellent agreement between ϕ_w^{calc} and ϕ_w^{fit} was obtained, typically ±5%, supporting the use of the model along with the method of calculating $\Delta\rho$ for this system. Note that the values of ϕ_w^{calc} were calculated by an accounting for the mutual solubilities of water and CO_2.[4]

TABLE 1: Results of Fits of the SANS Data at $W_o = 12.5$ to a Schultz Distribution of Polydisperse Spheres with an Ornstein−Zernicke Structure Factor

T (°C)	P (bar)	ϕ	ϕ_w^{calc}	ϕ_w^{fit}	R_w (Å)	$S(0)$	ξ (Å)
15	448	0.123	0.0455	0.0475	20.2	14.4	64.0
	379	0.121	0.0448	0.0463	20.4	11.9	58.4
	310	0.119	0.0439	0.0449	20.4	11.1	55.6
	241	0.116	0.0429	0.0444	20.7	11.1	58.5
	172	0.112	0.0416	0.0408	20.6	15.6	65.2
	138	0.110	0.0408	0.0389	20.3	26.0	82.4
	103[a]	0.107	0.0408	0.0199	20.4	11.4	41.5
25	379	0.118	0.0432	0.0477	20.3	8.20	51.3
	310	0.115	0.0423	0.0455	20.2	8.74	49.9
	241	0.112	0.0411	0.0427	20.1	11.2	54.9
	207	0.110	0.0403	0.0405	20.1	17.6	69.5
	172	0.107	0.0395	0.0372	19.4	30.2	81.8
	138[a]	0.104	0.0383	0.0137	18.8	16.0	36.5
35	379	0.114	0.0416	0.0445	19.4	6.98	44.4
	310	0.111	0.0405	0.0411	19.1	8.87	45.6
	241	0.107	0.0390	0.0375	18.8	16.5	59.9
	207	0.105	0.0382	0.0363	19.1	46.2	106
	172[a]	0.101	0.0370	0.0028	16.7	37.5	23.0
50	379	0.109	0.0389	0.0415	18.5	10.2	47.4
	345	0.107	0.0383	0.0402	18.7	12.6	54.0
	310	0.105	0.0376	0.0379	18.4	17.8	60.2
	283	0.103	0.0369	0.0347	18.1	37.7	85.9
	241[a]	0.100	0.0358	0.0166	18.0	17.9	45.3
65	379	0.107	0.0360	0.0355	17.5	17.6	54.1
	345	0.101	0.0352	0.0339	17.4	23.4	62.4
	328	0.100	0.0348	0.0328	17.2	52.4	93.4
	290[a]	0.097	0.0338	0.0152	17.4	17.4	43.1
80	379	0.098	0.0328	0.0301	16.4	39.0	72.0
	359	0.096	0.0323	0.0292	16.2	59.1	87.3
	324[a]	0.093	0.0319	0.0110	16.0	16.0	32.3
35	379	0.0515	0.0161	0.0161	17.6	7.46	20.0
	310	0.0501	0.0162	0.0179	17.9	7.70	31.7
	241	0.0482	0.0162	0.0171	17.8	10.7	37.6
50	379	0.0481	0.0153	0.0163	17.3	8.27	26.9
	345	0.0473	0.0153	0.0149	17.2	10.2	27.3
	310	0.0464	0.0154	0.0160	17.4	11.1	33.5
	276	0.0453	0.0154	0.0141	16.9	17.5	37.6
65	379	0.0445	0.0142	0.0145	16.0	10.4	25.7
	345	0.0436	0.0143	0.0107	15.2	18.6	26.0
	310	0.0424	0.0143	0.0149	16.5	14.2	35.6
80	379	0.0407	0.0128	0.0113	14.7	13.6	23.5
	345	0.0396	0.0129	0.0147	15.6	10.6	30.5

[a] Two-phase system, SANS performed on the upper phase.

As seen from Table 1, as the pressure is reduced approaching the cloud point at each temperature, $S(0)$ and ξ increase, indicating an increase in the size of the scattering centers and hence an increase in droplet interactions. As seen from Figure 2, decreasing the pressure moves the system closer to the critical point where droplet interactions are expected to be high. Recall that this increase in droplet attraction is evident by an increase in the low-Q scattering in Figures 3−8. Decreasing the pressure decreases the density and, thus, solvent power of CO_2, resulting in a decrease in solvent−surfactant tail interactions and a corresponding increase in tail−tail interactions until eventually a first-order phase transition results.[29,41] A similar increase in interactions due to a decrease in CO_2 density is observed as the temperature is increased at constant pressure. From Figure 1 it is evident that this increase in temperature at constant pressure also results in the system approaching the phase boundary where droplet interactions are expected to be high. Equivalently, the upper critical solution pressure seen in Figure 2 moves to higher pressures as the temperature is increased,[15] thus bringing the system closer to the critical point. The effect of droplet volume fraction on droplet interactions can be seen in Table 1 by comparing the lower entries at $\phi \sim 0.05$ to the upper entries at $\phi \sim 0.1$ at the same temperature and pressure. Decreasing the volume fraction decreases the values of $S(0)$ and ξ, indicating decreased droplet interactions as expected upon dilution.

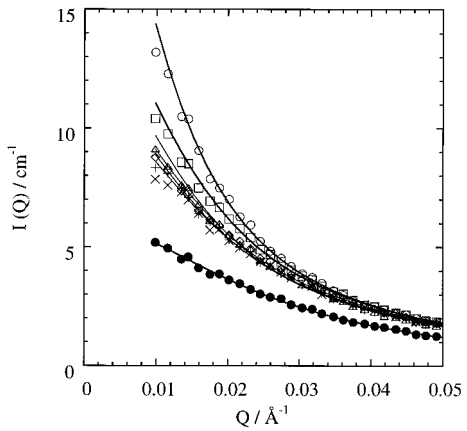

Figure 3. SANS scattering spectra at 15 °C, $W_o = 12.5$, and $S/C = 0.15$ at 449 (△), 380 (+), 311 (×), 242 (◇), 173 (□), 139 (○), and 104 (● two-phase) bar. Lines drawn represent the fit of the data to the polydisperse form factor, Ornstein−Zernicke structure factor model. Data for $Q > 0.05$ are not shown, as no variation was observed at large Q with pressure in the one-phase region.

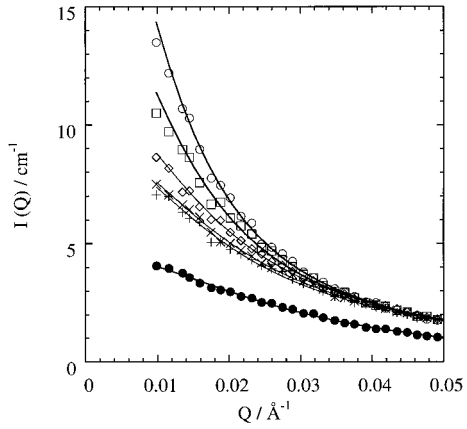

Figure 4. SANS scattering spectra at 25 °C, $W_o = 12.5$, and $S/C = 0.15$ at 380 (+), 311 (×), 242 (◇), 208 (□), 173 (○), and 139 (● two-phase) bar. See comments in Figure 3 caption.

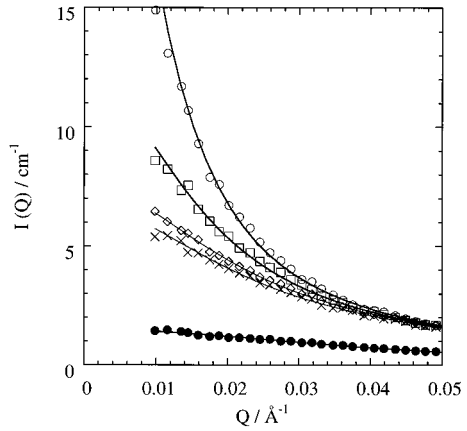

Figure 5. SANS scattering spectra at 35 °C, $W_o = 12.5$, and $S/C = 0.15$ at 380 (×), 311 (◇), 242 (□), 208 (○), and 173 (● two-phase) bar. See comments in Figure 3 caption.

The increase in droplet interactions in conventional oil-continuous systems has been attributed to overlap of the surfactant tails on neighboring droplets as solvent−tail interactions decrease. It has therefore been proposed that the interac-

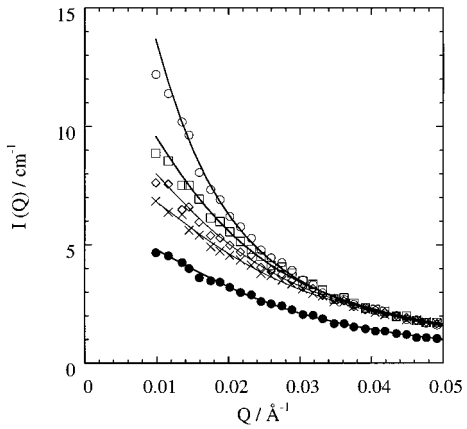

Figure 6. SANS scattering spectra at 50 °C, $W_o = 12.5$, and $S/C = 0.15$ at 380 (×), 346 (◇), 311 (□), 284 (○), and 242 (● two-phase) bar. See comments in Figure 3 caption.

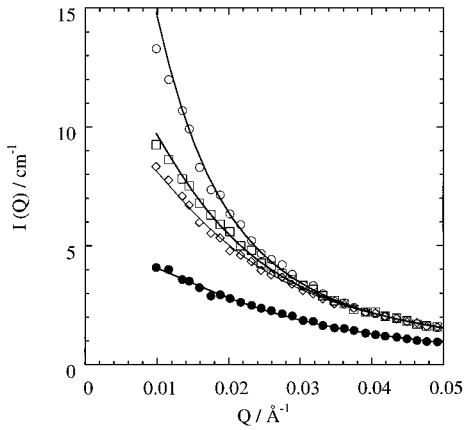

Figure 7. SANS scattering spectra at 65 °C, $W_o = 12.5$, and $S/C = 0.15$ at 380 (◇), 346 (□), 329 (○), and 291 (● two-phase) bar. See comments in Figure 3 caption.

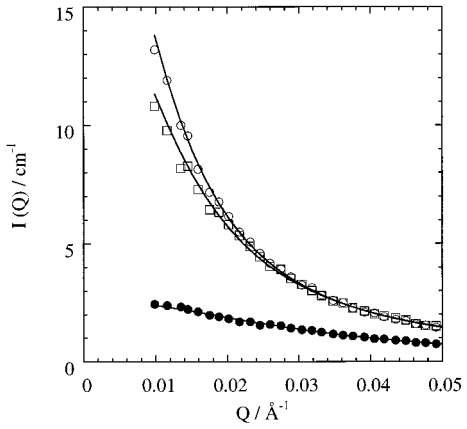

Figure 8. SANS scattering spectra at 80 °C, $W_o = 12.5$, and $S/C = 0.15$ at 380 (□), 360 (○), and 325 (● two-phase) bar. See comments in Figure 3 caption.

tions between microemulsion droplets whose centers are separated by a distance r can be represented by the Lemaire potential:[27,42]

$$U(r) = 0 \qquad \text{for } r > 2R_{HS} + l_p \tag{3a}$$

$$U(r) = -\Delta\rho k_B T V_o(r) \qquad \text{for } 2R_{HS} < r < (2R_{HS} + l_p) \tag{3b}$$

$$U(r) = \infty \qquad \text{for } r < 2R_{HS} \tag{3c}$$

where R_{HS} is the hard-sphere radius, $\Delta\rho$ is the difference in *atomic* density of the surfactant tails and the solvent, and $V_o(r)$ and l_P are the volume and distance of overlap of the surfactant tails. The Lemaire potential is difficult to apply directly to SANS data because $V_o(r)$ is a function of separation distance; however, Huang et al.[25,43] have demonstrated that the Lemaire potential can be accurately approximated by a square-well potential where $\Delta\rho k_B T V_o(r)$ is replaced with the square well depth ϵ (in units of $k_B T$). An analytical expression for the structure factor of a square-well potential has been derived,[44] making this potential particularly applicable to SANS data on microemulsion systems. Huang et al.[25] have demonstrated that the square-well depth determined from such a structure factor needs to be normalized as $\epsilon' = \ln(\epsilon + 1)$ to make it consistent with Monte Carlo simulations as well as measured values of the second virial coefficient.

In terms of the osmotic pressure Π, droplet interactions can be accounted for by adding a van der Waals-type attractive term accounting for droplet interactions[28,45] to the Carnahan−Starling hard-sphere equation of state:[46]

$$\Pi = \Pi_{HS} + \Pi_A = \frac{k_B T}{v_{HS}}\phi\frac{(1 + \phi + \phi^2 - \phi^3)}{(1 - \phi)^3} - \frac{k_B T}{v_{HS}}\frac{A}{2}\phi^2 \tag{4}$$

where $v_{HS} = {}^4/_3\pi R_{HS}^3$, ϕ is the droplet volume fraction, and the dimensionless interaction strength A is a function of drop size, temperature, and, for compressible solvents, pressure. It is related to the attractive potential $U_A(r)$, where $U_A(r)$ is the difference between the hard-sphere potential $U_{HS}(r)$ and $U(r)$, by the following equation:

$$A = \frac{4\pi}{k_B T}\frac{1}{v_{HS}}\int r^2\left[\exp\left(\frac{U_A(r)}{k_B T}\right) - 1\right] dr \tag{5}$$

For the square-well potential given in eq 3, $A = 8(\lambda^3 - 1)[\exp(\epsilon') - 1]$ where $\tau = (1 + l_p/2R_{HS})$. Note that the attractive term only accounts for two-body interactions, as evident from the ϕ^2 term in eq 4. From the criteria of the first and second derivative of the osmotic pressure equaling zero at the critical point, the van der Waals hard-sphere liquid model above gives a critical droplet volume fraction of $\phi_c = 0.13$ and a value of the interaction strength at the critical point of $A_c = 21.2$.

To further elucidate the effects of pressure and temperature on droplet interactions, the SANS data were fitted with a structure factor derived from the square-well potential.[44] The effects of polydispersity were ignored given the uncertainly in accurately representing the form and structure factors for a polydisperse square-well fluid.[47] The fit required four adjustable parameters, namely, the hard-sphere droplet volume fraction ϕ_{HS} and radius R_{HS}, the square well depth ϵ, and the penetration length l_p. However, ϕ_{HS} was calculated from the known overall droplet volume fraction by $\phi_{HS}/\phi = (R_{HS})^3/(R_{HS} + l_p)^3$.[48] This approach most likely represents a better approximation than assuming $\phi_{HS} = \phi_w$, as has been done previously.[49] Also, the overlap distance l_p in AOT systems has been shown to be approximately equal to the distance to the $-CH_2CH_3$ side chains of the surfactant tails.[43] Thus for PFPE-$COO^-NH_4^+$, l_p was calculated as the distance to the first $-CF_3$ side group, which from rotational isomeric state studies[50] is 3.9 Å. This assumption for the penetration length of PFPE-$COO^-NH_4^+$ seems realistic given the bulky nature of the $-CF_3$ group. Note that although the value of the regressed ϵ depended strongly on choice of l_p as λ is related to l_p, the resulting value of A was quite insensitive to the choice of l_p, changing only by about 1% as l_p was

TABLE 2: Results of Fits of the SANS Data at $W_o = 12.5$ and $S/C = 0.15$ to a Square-Well Potential Structure Factor with a Constant Overlap Distance ($l_P = 3.9$ Å)

T (°C)	P (bar)	ϕ_{HS}	R_{HS} (Å)	ϵ/k_BT	ϵ'	A	l_T (Å)
15	448	0.0866	31.0	12.1	2.57	19.1	14.7
	379	0.0850	30.9	11.8	2.55	18.9	14.3
	310	0.0833	30.8	11.7	2.54	18.7	14.3
	241	0.0812	30.7	11.9	2.55	19.1	13.8
	172	0.0785	30.6	12.4	2.60	20.0	13.9
	138	0.0764	29.9	12.8	2.63	21.4	13.5
	103[a]	0.0375	33.2	16.9	2.89	25.0	16.6
25	379	0.0825	30.6	11.1	2.49	17.9	14.1
	310	0.0805	30.5	11.3	2.51	18.2	14.2
	241	0.0778	30.1	11.7	2.54	19.2	13.9
	207	0.0758	29.5	12.8	2.63	20.7	13.3
	138[a]	0.0326	31.1	17.9	2.94	28.4	16.1
35	379	0.0782	28.6	10.2	2.42	17.8	13.1
	310	0.0760	28.5	10.6	2.45	18.5	13.3
	241	0.0727	27.9	11.7	2.54	20.7	13.0
	207	0.0707	27.7	12.7	2.62	22.8	12.5
	172[a]	0.0171	29.8	21.7	3.12	35.9	17.0
50	379	0.0742	28.2	10.9	2.48	19.2	13.5
	345	0.0730	28.3	11.3	2.51	19.7	13.4
	310	0.0684	28.6	12.2	2.58	21.2	14.0
	283	0.0690	26.9	12.3	2.59	22.8	12.7
	241[a]	0.0322	30.0	18.5	2.97	30.3	15.9
65	379	0.0692	26.9	11.3	2.51	20.9	13.3
	345	0.0673	26.5	11.8	2.55	22.2	12.9
	328	0.0658	25.8	12.3	2.58	23.8	12.4
	290[a]	0.0298	28.4	18.6	2.98	32.4	14.9
80	379	0.0636	24.9	11.9	2.55	23.8	12.4
	359	0.0620	24.4	12.0	2.57	24.7	12.1
	324[a]	0.0233	27.6	21.4	3.11	34.3	15.4

[a] Two-phase system, SANS performed on the upper phase.

increased by a factor of 2. Finally, as is typical for this type of model,[41,49] a vertical scale factor in $I(Q)$ of ±20% was allowed to account for inaccuracies in measuring the absolute intensity of scattering, as well as inaccuracies in the model, particularly the assumption of monodisperse droplets.

The results of the fits of the SANS data to the monodisperse square-well model are given in Table 2. The model fits were visually equivalent to those of the previous model in Figures 3−8 and, thus, are not shown. An exception occurs for $Q > 0.1$ Å^{-1}, where the monodisperse form factor exhibits values of zero. Since droplet interactions are manifested in the low-Q region, the uncertainty at high Q is not expected to have a significant effect on the results. Included along with the model fits are values of the surfactant tail length l_T calculated from the simple geometric criteria that $R_w + l_T = R_{HS} + l_p$, where R_w is determined from the model with the Ornstein−Zernicke structure factor, and R_{HS} is determined from the model with the square-well structure factor. The calculated values of l_T agree quite well with the value of 13 Å determined for water/PFPE-$COO^-NH_4^+$/PFPE−oil microemulsions from a phase diagram and geometric considerations (surfactant MW = 710 g/mol).[39] An exception to this agreement is observed below the cloud point (two-phase systems). This "closure" of the two models suggests that both models are reasonable in representing the behavior of these W/C microemulsion systems. The modest increase in R_{HS} and, thus, l_T in the two-phase region (note that R_w is essentially unchanged as the phase boundary is crossed, as seen in Table 1) may be the result of the formation of droplet clusters due to the large droplet attraction, which would effectively increase R_{HS}.

The effect of pressure and temperature on droplet interactions can be seen from the interaction strength A in Figure 9. Also shown are the electrical conductivity data for a similar H_2O/PFPE-$COO^-NH_4^+$/CO_2 microemulsion at $S/C = 0.18$. Except

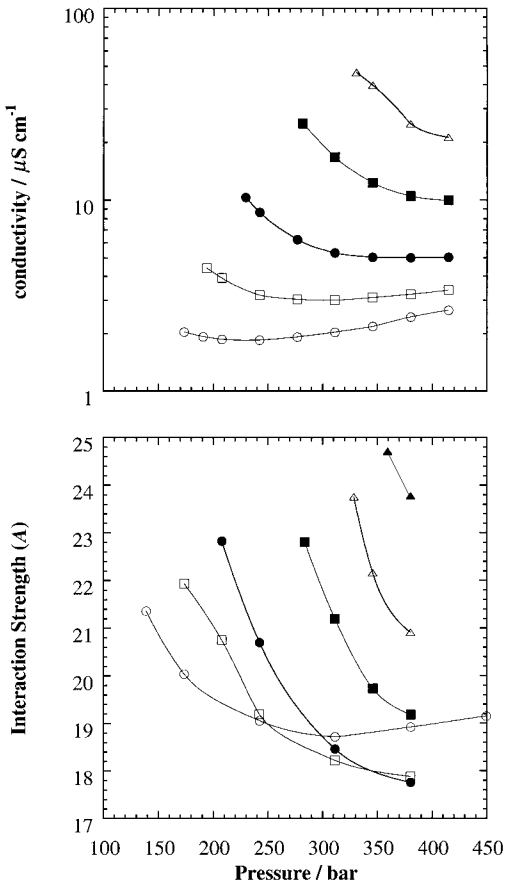

Figure 9. Electrical conductivity of H_2O/PFPE-$COO^-NH_4^+$/CO_2 microemulsions at $S/C = 0.18$ compared against the interaction strength of D_2O/PFPE-$COO^-NH_4^+$/CO_2 microemulsions at $S/C = 0.15$ determined from SANS. $T = 15$ (○), 25 (□), 35 (●), 50 (■), 65 (△), and 80 (▲) °C.

at 15 °C, droplet interactions and, thus, the values of the interaction strength A and electrical conductivity increase as the upper critical solution pressure (Figure 2) is approached. The upper critical solution pressure is approached with decreasing pressure at constant temperature or increasing temperature at constant pressure.

As the pressure is decreased at constant temperature, the value of A increases. As stated above, this increase in droplet attraction is a result of a decrease in solvent−tail interactions as the CO_2 solvent power is decreased, resulting in an increase in tail−tail interactions. This increase in tail−tail interactions gives rise to an increase in droplet interactions and a corresponding increase in droplet clustering. Droplet clustering allows for greater transport of ions between droplets and, thus, an increase in the electrical conductivity of the microemulsion. Similar effects of A on solvent power have been seen in the semicompressible water/AOT/near-critical propane system with a decrease in pressure,[41] as well as in water/AOT/alkane systems with an increase in alkane chain length.[49]

At the lowest temperature, both the conductivity and interaction strength go through a shallow minimum with pressure, which is a result of the system being close to both the upper and lower critical solution pressures, as seen in Figure 2.

Near the phase boundaries, the values of the interaction strength are close to the value predicted at the critical point, that is, $A_c = 21.2$ for a hard-sphere fluid with a van der Waals attractive term. As seen in Figure 2, all of the W/C microemulsions in this study are not that far from the critical point at phase separation. Likewise, the values of A are not that far from 21.2, with a minimum value of 18.

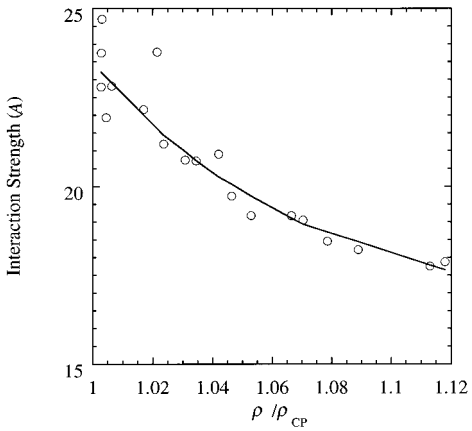

Figure 10. Interaction strength (A) versus the density of CO_2 divided by the density of CO_2 at the cloud point for $T > 15$ °C in the one-phase region.

The values of A exceed A_c at 35−80 °C as the pressure is reduced. This result may be expected since ϕ is slightly offset from the critical point at $\phi_c = 0.13$, and since the pressures are below the critical solution pressure.[51] For the water/AOT/octane system at $\phi < \phi_c$, A equals 22 near the phase transition, as is observed in Table 2.[25] Also, a value of $A > A_c$ could suggest three-body and higher interactions, due to the inability of CO_2 to sufficiently solvate the surfactant tails, resulting in stronger droplet interactions compared to conventional hydrocarbon systems. Furthermore, for a low-viscosity supercritical fluid like CO_2, multibody interactions may be expected to be more prevalent due to faster diffusion rates and, thus, an increase in droplet collisions. Indeed, in water/AOT/alkane microemulsions, percolation threshold volume fractions of as high as 0.7 have been observed,[52] while in water/PFPE-$COO^-NH_4^+$/CO_2 microemulsions the percolation threshold volume fraction was always less than 0.23.[15] The percolation at lower concentrations in W/C microemulsions again reflects tail−tail interactions resulting from limited tail solvation by CO_2.

The interaction strength A is also seen to increase as the temperature is increased from 35 to 80 °C at a constant pressure. This change is due in part to a decrease in the density of CO_2 as the temperature is increased. An increase in droplet interactions with temperature has also been observed in conventional water/AOT oil systems[53] and has been attributed to an inability of the solvent to pack with a favorable orientation in the surfactant tail region as temperature is increased.[28]

At high pressures, the opposite behavior occurs at the lowest two temperatures. As the temperature is decreased from 25 to 15 °C at $P > 310$ bar, the interaction strength increases as a result of the system approaching the lower critical solution pressure. This critical pressure moves to lower pressures as temperature is decreased, as seen in Figure 2.

An interesting observation is made when the interaction strength in the one-phase region is plotted versus the reduced density of CO_2, i.e., the actual density divided by the density at the cloud point (neglecting $T = 15$ °C, which is complicated by the lower critical solution pressure). As shown in Figure 10, the interaction strength is primarily a function of the reduced density of CO_2 and not temperature. Phase separation in these microemulsions results from the solvent leaving the tail region to raise the solvent volume and, thus, the entropy.[29,30] As the reduced density is lowered, a decrease in solvent−tail interactions results in an increase in tail−tail interactions as reflected in A. In contrast, changing the temperature at constant density has only a modest effect on the solvent power of CO_2 and the interaction strength.

A similar way of viewing solvent−tail interactions is by considering the complete Lemaire potential, where the normalized square well depth ϵ' is proportional to the density of the solvent. This potential is predicted to become zero as the *atomic* density of the solvent and surfactant tail become equal. From extrapolation of a series of isothermal linear plot of ϵ' vs CO_2 density, ϵ' would equal zero at an average CO_2 density of 1.87 g/cm^3 for 35−65 °C, (neglecting the low T results, where lower critical solution pressures occur, and the 80 °C results, where only two data points do not allow for legitimate linear fits). This density is close to the surfactant density of 1.8 g/cm^3,[39] indicating that the Lemaire potential for this system is applicable and that tail−tail interactions are the source of droplet interactions in W/C microemulsions. By coincidence, equal mass densities correspond to approximately equal atomic densities for CO_2 and the surfactant. Furthermore, for the range of temperatures in the present study, the density of CO_2 only reaches values of approximately 1.3 g/cm^3 at pressures as high as 3000 bar, well below the density of the surfactant.

The high values of A at the highest densities studied are in contrast to the water/AOT/near-critical propane system, where interaction strengths as low as 6.7 (calculated on the basis of the published ϵ' and λ values) were obtained at the highest densities.[41] Furthermore, a value of $A \sim 6.5$ was obtained in the water/AOT/nonane system.[28] These results suggest that droplet interactions may be more important in determining microemulsion stability in W/C systems, as compared to atmospheric pressure and near-critical alkane microemulsion systems. The strong interactions result from the relatively weak solvation of the surfactant tails by CO_2.

Another potential source of droplet interactions in W/C microemulsions is the van der Waals attractive force between the water cores. From the expression by Hamaker for the potential of the van der Waals force[54] and eq 5, the effective Hamaker constant (A_H^{eff}) for this system can be calculated from the interaction strength A by[45]

$$\frac{A_H^{\text{eff}}}{k_B T} = 2A\left(\frac{R_{HS}}{R_w}\right)^3\left[\frac{2}{3}\ln\frac{S_o - 2}{S_o + 2} - \frac{4}{3}S_o - \frac{1}{3}S_o^{\,3}\ln\frac{S_o^{\,2} - 4}{S_o^{\,2}}\right]^{-1} \quad (6)$$

where $S_o = 2R_{HS}/R_w$. From this expression, values of A_H^{eff} range from 500 to 800 k_BT in the one-phase region. In comparison, the value of the Hamaker constant for the interaction between the water cores calculated from a simplification of Lifshitz theory[55] is $1.9k_BT$ at 25 °C and 345 bar. This 2 orders of magnitude difference in the observed (from SANS, eq 6) and calculated (Lifshitz theory) Hamaker constant has been seen in several W/O microemulsions, indicating that droplet interactions between the water cores are negligible. Instead, tail−tail interactions must be the primary source of droplet interactions in W/C microemulsions.

As seen in Table 1, the fitted values of R_w are, within experimental error, independent of pressure at constant temperature. Similar results have been observed in other studies of water-in-supercritical fluid microemulsion systems.[3,4,12,13,41] The R_w values are comparable to the value of 20.2 Å obtained from SANS by Zielinski et al.[12] for a similar water/PFPE-COO^--NH_4^+/CO_2 system (surfactant MW = 695 g/mol) at $S/C = 0.02$ and $T = 35$ °C. For systems below the cloud-point pressure in Table 1, the R_w values in the upper phase of the microemulsions are, in general, similar to those obtained in the one-phase region at higher pressures. The droplet sizes are the same in the two phases, but concentrations are different as a result of droplet

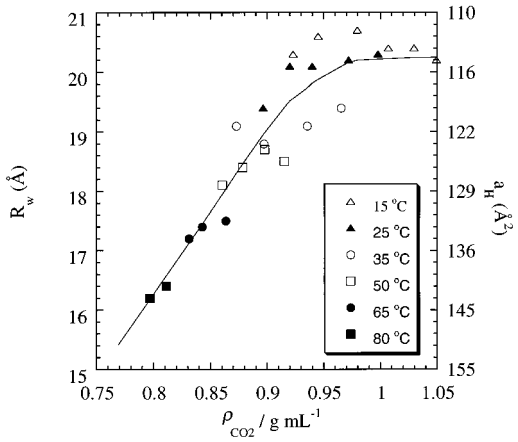

Figure 11. Plot of R_w and the corresponding a_H from eq 7 versus the density of CO_2 at each temperature.

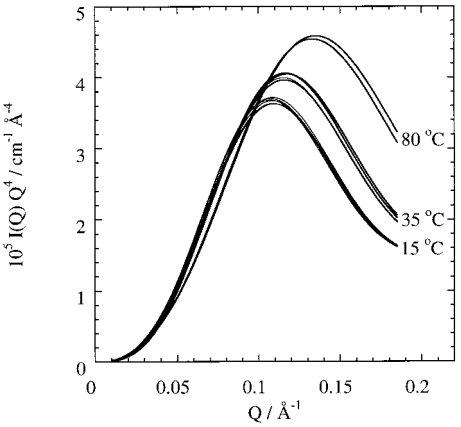

Figure 12. Porod plots versus temperature and pressure at $W_o = 12.5$ and $S/C = 0.15$. For clarity, only the model fits are shown; however, the data agreed well with the model, except at large Q. Note how pressure has little effect on the Porod plots at each temperature.

interactions, as has been observed in water/AOT/oil systems.[24] Also, decreasing the droplet volume fraction results in only a slight decrease in droplet size. Similar insensitivity in R_w with ϕ has been observed in conventional water/AOT/oil systems[24] due to the fact that R_w is primarily determined by W_o and the area per surfactant molecule at the oil−water interface).

In contrast to pressure, increasing the temperature results in a decrease in R_w, as shown in Figure 11. Simple geometric arguments lead to[24]

$$[1 + 2(\sigma/R^{avg})^2]R_w = \left(\frac{3v_w}{a_H}\right)W_o + \left(\frac{3v_H}{a_H}\right) \qquad (7)$$

where v_w is the molecular volume of water (D_2O), a_H is the area per surfactant molecule at the water−CO_2 interface, and v_H is the volume of the surfactant headgroup. From this equation, it is evident that a decrease in R_w at constant W_o must be accompanied by an increase in a_H. As temperature is increased, the thickness of the electric double layer increases, which may result in an increase in electrostatic repulsion between the surfactant headgroups and an increase in a_H. Interfacial tension measurements performed at the planar water−CO_2 interface with a similar PFPE-$COO^-NH_4^+$ surfactant (MW = 2500 g/mol) have also observed an increase in a_H from 76 to 107 Å^2 as the temperature was increased from 25 to 65 °C.[56]

In an attempt to further study the effect of temperature on a_H, Porod plots were generated. The limiting value of $I(Q)Q^4 = 2\pi(\Delta\rho)^2\Sigma$ at high Q, where Σ is the total surface area per volume in the system, was determined as seen in Figure 12. For systems where the surfactant concentration is much greater than the critical microemulsion concentration (cμc) of the surfactant, a_H can then be calculated as Σ divided by the surfactant molecular concentration. Unfortunately, the Q range employed in the present study did not allow for asymptotic values in the Porod plots in Figure 12 to be determined, due to the fact that the position of the first maximum and first minimum typically occurs at ~2.7/R and ~4.5/R, respectively. However, on the basis of the fact that the first maximum is shifted to higher values of $I(Q)Q^4$ as temperature is increased, these Porod plots suggest that the asymptotic values and, correspondingly, the values of a_H increase as temperature is increased. Furthermore, as temperature is increased the position of the first maximum is shifted to higher Q, indicating a decrease in drop size with increase in temperature, as was observed in Table 1.

In a previous study of dilute W/C microemulsions formed with a cationic PFPE-based surfactant, a similar tuning of droplet size with temperature was also observed. This was attributed to the partitioning of water from the water core of the microemulsion to the bulk CO_2 phase as a result of an increase in the solubility of water in CO_2 as temperature increased.[4] In the present study, however, the droplet concentration is sufficiently high such that solubility of water in CO_2 is insignificant (<1%) relative to the total amount of water in the system. Thus, partitioning of water is not expected to affect R_w. Therefore, the decrease in R_w in Figure 11 is most likely due to an increase in a_H as temperature is increased.

Conclusions

Droplet interactions in water-in-carbon dioxide microemulsions near the critical volume fraction $\phi_c = 0.13$ have been measured quantitatively with small-angle neutron scattering (SANS). Two models for the structure factor (Ornstein−Zernicke and square-well) are shown to accurately represent the experimental SANS data and many of the salient physical features of water-in-CO_2 microemulsions. Droplet interactions increase as the upper critical solution pressure is approached with decreasing pressure at constant temperature, increasing temperature at constant pressure, or increasing droplet volume fraction as evidenced by an increase in the structure factor at zero momentum vector, $S(0)$, the correlation length, ξ, and the square-well depth. This increase in droplet interactions is a result of the decrease in solvent−tail interactions and a corresponding increase in tail−tail interactions. Even well above the upper critical solution pressure, the interaction strength A exceeds the value for water-in-alkane microemulsions, reflecting limited solvation of the surfactant tails by CO_2. This large A indicates that it is more difficult to overcome droplet interactions to produce stable microemulsions in CO_2. At low temperatures the appearance of a lower critical solution pressure results in an increase in droplet interactions as the pressure is raised or lowered. Near both the upper and lower critical points, the interaction strength determined from the SANS data approaches the value predicted at the critical point for a hard-sphere fluid with a van der Waals attractive term. Pressure and volume fraction have a negligible effect on the droplet size. However, as temperature is increased, an increase in surface area per surfactant molecule at the interface and a corresponding increase in drop size resulted from an increase in the thickness of the electric double layer and, thus, repulsion between surfactant headgroups. The surfactant tail length, estimated to be 13 Å by comparing the regressed parameters of the two models, agrees

with experimental and theoretical values, indicating that both models accurately describe this system.

Acknowledgment. We acknowledge support from the U.S. Department of Energy (DE-FG03-96ER14664), the Texas Advanced Technology Program, the Welch Foundation, and the Separations Research Program at the University of Texas. Participants from Oak Ridge National Laboratory and the University of Tennessee were supported by the Divisions of Materials Sciences and Chemical Sciences of the U.S. Department of Energy. The research at Oak Ridge was supported by the U.S. Department of Energy under Contract DE-AC05-00OR22725 with the Oak Ridge National Laboratory, managed by UT-Battelle, LLC. We also thank R. Triolo for helpful discussions.

References and Notes

(1) Harrison, K.; Goveas, J.; Johnston, K. P.; O'Rear, E. A. *Langmuir* **1994**, *10*, 3536−3541.
(2) Johnston, K. P.; Harrison, K. L.; Clarke, M. J.; Howdle, S. M.; Heitz, M. P.; Bright, F. V.; Carlier, C.; Randolph, T. W. *Science* **1996**, *271*, 624−626.
(3) Eastoe, J.; Cazalles, B. M. H.; Steytler, D. C.; Holmes, J. D.; Pitt, A. R.; Wear, T. J.; Heenan, R. K. *Langmuir* **1997**, *13*, 6980−6984.
(4) Lee, C. T.; Johnston, K. P.; Dai, H. J.; Cochran, H. D.; Melnichenko, Y. B.; Wignall, G. D. *J. Phys. Chem. B* **2000**, *104*, 11094−11102.
(5) Lee, C. T.; Psathas, P. A.; Johnston, K. P. *Langmuir* **1999**, *15*, 6781−6791.
(6) Jacobson, G. B.; Lee, C. T.; Johnston, K. P. *J. Org. Chem.* **1999**, *64*, 1201−1206.
(7) Jacobson, G. B.; Lee, C. T.; daRocha, S. R. P.; Johnston, K. P. *J. Org. Chem.* **1999**, *64*, 1207−1210.
(8) Jacobson, G. B.; C. Ted Lee, J.; Johnston, K. P.; Tumas, W. *J. Am. Chem. Soc.* **1999**, *121*, 11902−11903.
(9) Clarke, M. J.; Harrison, K. L.; Johnston, K. P.; Howdle, S. M. *J. Am. Chem. Soc.* **1997**, *119*, 6399−6406.
(10) Ji, M.; Chen, X.; Wai, C. M.; Fulton, J. L. *J. Am. Chem. Soc.* **1999**, *121*, 2631−2632.
(11) Holmes, J. D.; Bhargava, P. A.; Korgel, B. A.; Johnston, K. P. *Langmuir* **1999**, *15*, 6613−6615.
(12) Zielinski, R. G.; Kline, S. R.; Kaler, E. W.; Rosov, N. *Langmuir* **1997**, *13*, 3934−3937.
(13) Eastoe, J.; Bayazit, Z.; Martel, S.; Steytler, D. C.; Heenan, R. K. *Langmuir* **1996**, *12*, 1423−1224.
(14) Salaniwal, S.; Cui, S. T.; Cummings, P. T.; Cochran, H. D. *Langmuir* **1999**, *15*, 5188−5192.
(15) Lee, C. T.; Bhargava, P.; Johnston, K. P. *J. Phys. Chem. B* **2000**, *104*, 4448−4456.
(16) Bhattacharya, S.; Stokes, J. P.; Kim, M. W.; Huang, J. S. *Phys. Rev. Lett.* **1985**, *55*, 1884−1887.
(17) Boned, C.; Peyrelasse, J.; Saidi, Z. *Phys. Rev. E* **1993**, *47*, 468−478.
(18) Chen, S. H.; Rouch, J.; Sciortino, F.; Tartaglia, P. *J. Phys.: Condens. Matter* **1994**, *6*, 10855−10882.
(19) de Gennes, P. G. *J. Phys. (Paris)* **1980**, *41*, C3−17.
(20) Iezzi, A.; Enick, R.; Brady, J. In *Supercritical Fluid Science and Technology*; Johnston, K. P., Penninger, J. M. L., Eds.; ACS Symposium Series 406; American Chemical Society: Washington, DC, 1989; pp 122−139.
(21) Oates, J. Ph.D. Dissertation, University of Texas, Austin, TX, 1989.
(22) Consani, K. A.; Smith, R. D. *J. Supercrit. Fluids* **1990**, *3*, 51−65.
(23) Kotlarchyk, M.; Chen, S.-H.; Huang, J. S. *Phys. Rev. A* **1983**, *28*, 508−511.
(24) Kotlarchyk, M.; Chen, S.-H.; Huang, J. S.; Kim, M. W. *Phys. Rev. A* **1984**, *29*, 2054−2069.
(25) Huang, J. S.; Safran, S. A.; Kim, M. W.; Grest, G. S.; Kotlarchyk, M.; Quirke, N. *Phys. Rev. Lett.* **1984**, *53*, 592−595.
(26) Chen, S. H. *Annu. Rev. Phys. Chem.* **1986**, *37*, 351−399.
(27) Lemaire, B.; Bothorel, P.; Roux, D. *J. Phys. Chem.* **1983**, *87*, 1023−1028.
(28) Huang, J. S. *J. Chem. Phys.* **1985**, *82*, 480−484.
(29) Peck, D. G.; Johnston, K. P. *J. Phys. Chem.* **1991**, *95*, 9549−9556.
(30) Peck, D. G.; Johnston, K. P. *J. Phys. Chem.* **1993**, *97*, 5661.
(31) da Rocha, S. R. P.; Harrison, K. L.; Johnston, K. P. *Langmuir* **1999**, *15*, 419−428.
(32) Koehler, W. C. *Physica* **1986**, *137B*, 320−329.
(33) Wignall, G. D.; Bates, F. S. *J. Appl. Crystallogr.* **1987**, *20*, 28−40.
(34) Kotlarchyk, M.; Chen, S.-H. *J. Chem. Phys.* **1983**, *79*, 2461−2469.
(35) Gradzielski, M.; Langevin, D.; Farago, B. *Phys. Rev. E* **1996**, *53*, 3900−3919.
(36) Teubner, M. *J. Chem. Phys.* **1991**, *95*, 5072−5081.
(37) Zulauf, M.; Eicke, H.-F. *J. Phys. Chem.* **1979**, *83*, 480−486.
(38) Wiebe, R.; Gaddy, V. L. *J. Am. Chem. Soc.* **1939**, *61*, 315−318.
(39) Chittofrati, A.; Lenti, D.; Sanguineti, A.; Visca, M.; Gambi, C. M. C.; Senatra, D.; Zhou, Z. *Prog. Colloid Polym. Sci.* **1989**, *79*, 218−225.
(40) Wiebe, R.; Gaddy, V. L. *Chem. Rev.* **1941**, *63*, 475−477.
(41) Kaler, E. W.; Billman, J. F.; Fulton, J. L.; Smith, R. D. *J. Phys. Chem.* **1991**, *95*, 458−462.
(42) Roux, D.; Bellocq, A. M.; Bothorel, P. In *Surfactants in Solution*; Mittal, K. L., Lindman, B., Eds.; Plenum Press: New York, 1984; Vol. 3, pp 1843−1865.
(43) Huang, J. S.; Kim, M. W. In *Physics of Amphiphiles: Micelles, Vesicles and Microemulsions*; Degiorgio, V., Corti, M., Eds.; North-Holland Physics Publishing: Amsterdam, 1985; pp 864−875.
(44) Sharma, R. V.; Sharma, K. C. *Physica* **1977**, *89A*, 213-218.
(45) Agterof, W. G. M.; Zomeren, J. A. J. V.; Vrij, A. *Chem. Phys. Lett.* **1976**, *43*, 363−367.
(46) Carnahan, N. F.; Starling, K. E. *J. Chem. Phys.* **1969**, *51*, 635.
(47) Bergenholtz, J.; Romagnoli, A. A.; Wagner, N. J. *Langmuir* **1995**, *11*, 1559−1570.
(48) Cazabat, A. M.; Langevin, D.; Pouchelon, A. *J. Colloid. Interface Sci.* **1980**, *73*, 1.
(49) Billman, J. F.; Kaler, E. W. *Langmuir* **1990**, *6*, 611−620.
(50) Hamada, T. *Phys. Chem. Chem. Phys.* **2000**, *2*, 115−122.
(51) Safran, S. A.; Turkevich, L. A. *Phys. Rev. Lett.* **1983**, *50*, 1930−1933.
(52) Cametti, C.; Codastefano, P.; Tartaglia, P.; Chen, S.-H.; Rouch, J. *Phys. Rev. A* **1992**, *45*, R5358−R5361.
(53) Huang, J. S.; Kim, M. W. *Phys. Rev. Lett.* **1981**, *47*, 1462−1465.
(54) Hamaker, H. C. *Physica IV* **1937**, 1058−1072.
(55) Israelachvili, J. *Intermolecular & Surface Forces*, 2nd ed.; Academic Press: San Diego, CA, 1992.
(56) da Rocha, S. R. P.; Johnston, K. P. *Langmuir* **2000**, *16*, 3690−3695.